Deflating the RNA Mg^{2+} bubble. Stereochemistry to the rescue!

Pascal Auffinger[1]*, Eric Ennifar[1] and Luigi D'Ascenzo[2]

[1] Architecture et Réactivité de l'ARN, Université de Strasbourg, Institut de Biologie Moléculaire et Cellulaire du CNRS, Strasbourg, 67084, France

[2] Department of Integrative Structural and Computational Biology, The Scripps Research Institute, La Jolla, CA 92037, USA

* To whom correspondence should be addressed. Tel: +33 388 41 70 49; Fax: +33 388 60 22 18;
Email: p.auffinger@ibmc-cnrs.unistra.fr

Abstract

Proper evaluation of the ionic structure of biomolecular systems remains challenging in X-ray and cryo-EM techniques. Herein, we re-evaluate the model of the ribosome ionic structure proposed in a 2019 Nat. Commun. paper by A. Rozov et al. We establish that neglecting stereochemical principles when evaluating ion binding features, even when K^+ anomalous signals are available, results in misleading conceptions of the solvent structure of ribosomal particles. We propose an alternative interpretation of the crystallographic data that suggests that monovalent ions and not divalent ions are prevalent in the 1st solvation shell of ribosomes. We stress that the use of proper stereochemical guidelines is critical for deflating the current Mg^{2+} bubble witnessed in many ribosome and eventually in other RNA structures.

A recent publication by Rozov, Yusupova et al. (Rozov et al. 2019), emphasized that long-wavelength X-ray diffraction techniques can now be used to detect the presence of potassium ions (K^+) in large ribosome structures counting >150.000 heavy atoms. This accomplishment involved the use of the dedicated I23 *in-vacuum* long-wavelength beamline at the Diamond Light Source facility (Wagner et al. 2016) to detect the anomalous signal of this biologically essential cation (Epstein 2003; Nierhaus 2014; Auffinger et al. 2016; Danchin and Nikel 2019). These experiments allowed Rozov et al. to revisit the ribosome ionic structure proposing that electron density patterns, previously attributed to Mg^{2+}, can now safely be associated with K^+ when coordination distances and geometries command it, as demonstrated earlier through the use of candid stereochemically based methods (Leonarski et al. 2017; Leonarski et al. 2019). Precisely, the authors focused on the role of K^+ at the decoding center, showing that a monovalent ion acts as a structural link between the protein uS12, the mRNA codon and the rRNA.

Correct ion identification is of importance since the modeling of a weakly coordinating K^+ (chaotropic) versus a more organizing and stabilizing Mg^{2+} (kosmotropic) ion at the decoding center or elsewhere in ribosomes has profound implications on how we picture the internal dynamics, folding and assembly of these particles. For instance, a monovalent ion should facilitate rather than hinder the shift of tRNAs and mRNAs from one binding site to the other since the residency times of water molecules coordinating to K^+ and Mg^{2+} in aqueous solution are estimated to be, respectively, below 10 ps and in the microsecond range (Bleuzen et al. 1997; Joung and Cheatham 2009). The residency times of Mg^{2+} bound to three phosphate groups as observed in the rRNA core (Klein et al. 2004) may even be longer and possibly equal the lifetime of the folded ribosomal subunits. Thus, the presence of Mg^{2+} in the decoding center is unlikely since this ion might “grip” the translational machinery by establishing disproportionately strong contacts between the various molecular partners.

To improve our understanding of ion binding features, it is essential to get a coherent estimate of the balance of monovalent and divalent ions and of their position in nucleic acids. By precisely examining the Rozov et al. 70S elongation complex structure (PDBid: 6QNR), one could conclude that Mg^{2+} (1005 ions) and not K^+ (367 ions), dominates the ribosomal ionic landscape. Herein, we challenge this crystallographic data interpretation through the use of straightforward stereochemical principles. We propose that K^+ and not Mg^{2+} is the prevalent ion in the 1st solvation shell of ribosomes.

The dynamical differences between bound K^+ and Mg^{2+} are a direct consequence of the ion stereochemistry that has been repeatedly described (Harding et al. 2010; Bowman et al. 2012; Zheng et al. 2014; Leonarski et al. 2017; Leonarski et al. 2019). In short, the main distinctive character of these ions, besides their charge, resides in their idiosyncratic coordination distances (Mg^{2+}: ≈2.1 Å; K^+: ≈2.8 Å; **Figure 1**). Such differences make them difficult to misidentify even in medium resolution structures (≈3.0 Å). The second major discriminating factor is related to the strict octahedral coordination of Mg^{2+} that is rarely adopted by K^+. The latter ion, given its larger ionic radius, prefers binding modes with coordination numbers of 7 to 8, such as for example square anti-prismatic —see UCSF Chimera definition (Pettersen et al. 2004). These binding modes are recurrently observed in potassium channels, nucleic acid quadruplexes and other RNA systems (Zhou et al. 2001; Auffinger et al. 2016; Leonarski et al. 2017).

K^+ and Mg^{2+} have also distinct binding preferences (Leonarski et al. 2017; Leonarski et al. 2019). The primary ligands for monovalent ions in nucleic acids are nucleobase carbonyl groups (Leonarski et al. 2019). As such, the major groove of G•U pairs has recurrently been found to constitute an excellent binding location for K^+ but not for Mg^{2+} ions (Klein et al. 2004; Fan et al. 2005; Wang et al. 2009; Leonarski et al. 2019; Westhof et al. 2019). On the other hand, Mg^{2+} prefers binding to phosphate and carboxyl groups and rarely binds to nitrogen atoms or to carbonyl, ester and hydroxyl oxygen atoms (Leonarski et al. 2017; Leonarski et al. 2019). Thus, in the absence of phosphate or carboxylate coordination, Mg^{2+} assignments have to be supported by robust stereochemical evidence.

With this in mind, it has probably not escaped readers of the original publication that the experiments designed by Rozov et al. to assign K^+ are technically demanding. Therefore, one may wonder if equivalent results could have been obtained by simpler techniques that are based on a rigorous application of stereochemical rules (Leonarski et al. 2017; Handing et al. 2018; Leonarski et al. 2019). For us, the answer is "Yes".

A rapid screen of the 3.1 Å resolution 6QNR structure (Rozov et al. 2019) shows, as expected, a 1st broad K^+ coordination peak centered around 2.8 Å (**Figure 1a**) (Leonarski et al. 2017; Leonarski et al. 2019). Therefore, none of the solvent density peaks with coordination distances around 2.8 Å should have been associated with Mg^{2+} in the initially released 4V6F structure that embeds a record-breaking 5345 assigned divalent ions (Jenner et al. 2010). As an illustration, Figure 2 of the Rozov et al. paper, Figure 8 of a related publication that analyzed the parent 5E81 structure (Leonarski et al. 2019) and **Figures 1d/S1** show that stereochemical considerations should have been sufficient to completely rule out an Mg^{2+} assignment for density peaks close to the decoding center and, instead, should have led to the more sensible and stereochemically correct placement of K^+, even in the absence of an anomalous signal. The assignment of other solvent particles with coordination distances around 2.8 Å is easily discarded since water molecules cannot be observed in structures with resolutions >3.0 Å and would not display density peaks as high as those of K^+. Furthermore, in the aforementioned figures, it is clear that the ion coordination geometry is not compatible with a water molecule or a tetrahedral NH_4^+ while the observed non-octahedral coordination pattern disqualifies Mg^{2+} immediately.

These observations challenge an assumption made by Rozov et al. suggesting that at resolutions around 3.0 Å, it is almost impossible to distinguish K^+ from Mg^{2+} based on average M^{n+}…N/O coordination distances. We suggest that stereochemically based K^+ assignments and Mg^{2+} assignments are possible. To assess our point, we visualized all 6QNR ions in the Coot and UCSF Chimera visualization programs (Pettersen et al. 2004; Emsley et al. 2010) and checked regular and anomalous difference maps. We also developed an 'in-house' analysis program to screen the stereochemistry of the assigned ions (Leonarski & Auffinger, unpublished; **Supplementary Information**). These combined checks confirmed that none of the assigned K^+ in 6QNR could have been mistaken for Mg^{2+} given coordination distances around 2.8 Å and the absence of associated octahedral coordination patterns. Yet, we isolated a few borderline K^+ assignments in 6QNR. For instance, 12 K^+ have no 1st coordination shell, i.e., no ligand coordination distances below 3.4 Å. For some density patterns associated with these ions, the presence of an anomalous signal not overlapping with the ion position in the $2F_o$-F_c map does not warrant a clear-cut K^+ assignment

(**Figure S2**). Instead, it suggests the occurrence of local structural differences in the solvent and in the ion binding site organization between the 10 years old original crystals and the recent batch of four crystals used for the anomalous signal detection.

While the main focus of Rozov et al. was the identification of 367 K^+, the authors revised also the placement of Mg^{2+} that resulted in the assignment of 1005 Mg^{2+} in 6QNR versus 5345 Mg^{2+} in 4V6F (Jenner et al. 2010). As for now, it has been almost impossible, besides a single documented exception, to collect anomalous signals for Mg^{2+} in macromolecular systems (Liu et al. 2013). Precise Mg^{2+} assignments necessitate a resolution around 2.4 Å or better that allows the observation of a well-defined octahedral coordination shell with coordination distances ≈2.1 Å (**Figure S3**). In 6QNR, no Mg^{2+} octahedral density patterns were observed (**Figure 2c**). Nonetheless, a hydration sphere has been modeled for 393 out of 1005 Mg^{2+}. Regrettably, these hydration spheres generate a large number of clashes involving Mg^{2+} coordinating water molecules as listed in both the publicly available PDB validation report and the output of our analysis program (**Supplementary Information**). A rapid screen of the water oxygen atom to rRNA and r-protein oxygen atom distances reveals the presence of 564 water contact distances below 2.4 Å, affecting 321 Mg^{2+} (82% of the 393 hydrated Mg^{2+}; **Figure 2**). This observation is significant since it has been clearly established that hydrogen bonds shorter than 2.4–2.5 Å are artefactual (Kruse et al. 2019). In 6QNR, such short contacts reveal that Mg^{2+} hydration spheres and sometimes entire ion binding sites, have been poorly modeled and that other mono- or divalent ions or solvent molecules could be present at these locations. For instance, the ion shown in **Figure 2** is at ≈2.8 Å of an oxygen atom of a phosphate group and is, therefore, more likely K^+ despite the lack of reported anomalous signal.

In total, we identified 853 out of a total of 1005 Mg^{2+} (≈85%) that do not satisfy all requested stereochemical criteria necessary for unambiguous ion assignments (**Supplementary Information**). Among those, 138 and 361 Mg^{2+} display at least one coordination distance that respectively suggests the presence of Na^+ or K^+. In addition, 144 Mg^{2+} have no atoms in their 1st coordination shell rendering any conclusive identification impossible. Of course, in the absence of stereochemical evidence, some of the latter density spots could correspond to $Mg(H_2O)_6^{2+}$ but could as well correspond to buffer solvent molecules. Therefore, any ion assignment at those locations remains a perilous three-dimensional gambling exercise that is further hampered by locally inaccurate structural modeling. For instance, within medium to low resolution structures, assigning K^+ or Mg^{2+} with occupancies of 0.5 should clearly be avoided; 24 ions with partial occupancies are present in 6QNR.

Less dramatic but not to be neglected, we evidenced through a simple distance check the use of an "idealized" average Mg^{2+}…OH_2 distance of 2.18 ± 0.02 Å (far from the 2.0 Å mentioned in Figure 2 of Rozov et al.) that contrasts with the known coordination distances of water to Mg^{2+} that genuinely turns around 2.06±0.03 Å as shown in **Figures 1/3** (Leonarski et al. 2017; Leonarski et al. 2019). Such errors can easily become viral (Minor et al. 2016) and may confuse, among others, untrained scientists that lack time to fix stereochemical issues.

To summarize, our survey suggests that roughly 80% of the 1005 Mg^{2+} are misassigned or suffer from severe stereochemical issues and that ≈400 of these Mg^{2+} are Na^+ or K^+. This number adds to the 361 K^+ that were assigned based on anomalous signals suggesting the presence of ≈700-800 monovalent ions and ≈200 Mg^{2+} in the 6QNR structure (or ≈400 monovalent ions and ≈100 Mg^{2+} in the

ribosomal 1st solvation shell since the 6QNR crystallographic unit comprises two ribosomal particles). At a 3.1 Å resolution, these numbers can only be qualitative. However, we believe that the proposed orders of magnitude are representative of the balance of mono- and divalent ions in 1st solvation shell of ribosomes.

At this point, we note that the number of assigned ions is only able to neutralize about 1/5 to 1/4th of the negative charge carried by ribosomes suggesting that the ionic atmosphere is essentially composed of non-coordinating ions that remain undetected by X-ray or cryo-EM techniques. Given the much larger K^+ over Mg^{2+} concentration *in crystallo* but also *in vivo*, it is not unreasonable to state that K^+, along with polyamines (Nierhaus 2014; Miller-Fleming et al. 2015; Noeske et al. 2015), is responsible for the largest part of the charge neutralization of ribosomes while Mg^{2+} intervenes at a limited number of strategic locations to stabilize intricate structural folds (Bowman et al. 2012). This conclusion is not a surprise if we consider that Mg^{2+} is a regulated resource in the cell that is used with parsimony and for specific structural purposes while K^+ is highly abundant (Nierhaus 2014; Auffinger et al. 2016; Danchin and Nikel 2019). It is more of a surprise that the concerned structural community did not challenge unwarranted Mg^{2+} assignments that have been violating stereochemical rules for so long. If the Rozov et al. along with the earlier Klein and Steitz structures (Klein et al. 2004) and other studies (Leonarski et al. 2017; Leonarski et al. 2019) add to our knowledge of the monovalent ion binding to nucleic acids and corrects previous stereochemically incorrect assignments (Jenner et al. 2010), these structures certainly continue to mask essential Mg^{2+} binding features.

Although numerous ribosomal structures with deficient ion placements have been deposited to the PDB, none of those placed a strong emphasis on the ribosome ionic structure besides a seminal study by Klein and Steitz (Klein et al. 2004). The latter were the first authors to identify monovalent ions around a ribosomal subunit. However, in most instances, ions were placed in X-ray structures by using automatic routines to improve crystallographic statistics (Shabalin et al. 2018). Sometimes, equivalent strategies are used during the refinement of cryo-EM structures and led similarly to locally deficient ion placements. In a recently published 50S *Staphylococcus aureus* cryo-EM structure at 3.2 Å resolution (PDBid: 6SJ6), the authors reported the use of the *Thermus thermophilus* 6QNR structure discussed herein to model K^+. They mentioned that densities that can be attributed to solvent molecules have been interpreted as Mg^{2+} (Khusainov et al. 2020). As a result, the 6SJ6 model deposited to the PDB contains 3 K^+, 56 Mg^{2+} and no water molecules. Surprisingly, the number of K^+ and Mg^{2+} is well below the number of ions expected for a bacterial 50S subunit. To verify these assignments, we used our in-house diagnosis program on this structure and found that only 14 out of 56 ions satisfy requested stereochemical criteria. In 6SJ6, no octahedral density patterns could be observed around Mg^{2+}. A visual inspection of ion positions and density maps led to the conclusion that almost none of these ions were appropriately assigned (**Figure 4**). Therefore, we suggest that in the absence of clear experimental and stereochemical evidence, it may be more suitable to not assign any ions in biomolecular structures with inappropriate resolutions since those assignments may subsequently be taken for granted by others with the risk to create inappropriate prior knowledge subsequently affecting the outcome of database surveys (Minor et al. 2016).

It is now appreciated that ribosomes like any other biomolecular system cannot fulfill their functions without the presence of a finely tuned ion and solvent ecosystem. Thus, besides a correct K^+ and Mg^{2+}

identification, the real challenge is to disentangle the structural and functional roles these ions assume. For that, gathering high-resolution X-ray and cryo-EM data remains the best option for promoting our understanding of mono- and divalent ion binding features when coupled with proper stereochemical knowledge. Collecting anomalous signals, among other important ion identification strategies (Hare et al. 2015; Grime et al. 2020), will complement the above and will contribute to 'deflate' the Mg^{2+} bubble currently witnessed in numerous ribosomal structures, a bubble that eventually affects also a significant part of structures in the RNA world as we know it (Leonarski et al. 2017; Leonarski et al. 2019). Yet, for light ions present in crystallization buffers such as Mg^{2+}, Na^{+}, NH_4^{+}, …, anomalous signals cannot be collected. Stereochemistry remains the only viable option to precisely identify and locate them.

‡

Acknowledgment

We thank Alexey Rozov for having provided the anomalous diffraction data and Filip Leonarski for having provided an early version of his “Ion Report” program for the analysis of the ribosomal ionic environment. We thank Philippe Dumas, Quentin Vicens, and Filip Leonarski for critical views on the manuscript.

Author contributions

PA conceived the project. PA, EE, and LD analyzed the data. LD helped in writing analysis tools. PA wrote the manuscript. All authors discussed the results and conceived the final manuscript.

Additional information

Supplementary Information accompanies this publication.

It consists in two parts: the first contains methodological details, one table and six figures; the second and third, a full output of our “Ion_diagnosis” program for the 6QNR and 6SJ6 structures.

Competing interests. None.

References

Auffinger P, D'Ascenzo L, Ennifar E. 2016. Sodium and potassium interactions with nucleic acids. *Met. Ions Life Sci.* **16**: 167-201.

Bleuzen A, Pittet PA, Helm L, Merbach AE. 1997. Water exchange on magnesium(II) in aqueous solution: a variable temperature and pressure ^{17}O NMR study. *Magn. Reson. Chem.* **35**: 765-773.

Bowman JC, Lenz TK, Hud NV, Williams LD. 2012. Cations in charge: magnesium ions in RNA folding and catalysis. *Curr. Opin. Struct. Biol.* **22**: 262-272.

Danchin A, Nikel PI. 2019. Why Nature chose potassium. *J. Mol. Evol.* **87**: 271-288.

Emsley P, Lohkamp B, Scott WG, Cowtan K. 2010. Features and development of Coot. *Acta Cryst.* **D66**: 486-501.

Epstein W. 2003. The roles and regulation of potassium in bacteria. *Prog. Nucleic Acid. Res. Mol. Biol.* **75**: 293-320.

Fan Y, Gaffney BL, Jones RA. 2005. RNA GG x UU motif binds K^+ but not Mg^{2+}. *J. Am. Chem. Soc.* **127**: 17588-17589.

Grime GW, Zeldin OB, Snell ME, Lowe ED, Hunt JF, Montelione GT, Tong L, Snell EH, Garman EF. 2020. High-throughput PIXE as an essential quantitative assay for accurate metalloprotein structural analysis: development and application. *J. Am. Chem. Soc.* **142**: 185-197.

Groom CR, Bruno IJ, Lightfoot MP, Ward SC. 2016. The Cambridge Structural Database. *Acta Cryst.* **B72**: 171-179.

Handing KB, Niedzialkowska E, Shabalin IG, Kuhn ML, Zheng H, Minor W. 2018. Characterizing metal-binding sites in proteins with X-ray crystallography. *Nat. Protoc.* **13**: 1062-1090.

Harding MJ, Nowicki MW, Walkinshaw MD. 2010. Metals in protein structures: a review of their principal features. *Cryst. Rev.* **16**: 247-302.

Hare DJ, New EJ, de Jonge MD, McColl G. 2015. Imaging metals in biology: balancing sensitivity, selectivity and spatial resolution. *Chem. Soc. Rev.* **44**: 5941-5958.

Jenner LB, Demeshkina N, Yusupova G, Yusupov M. 2010. Structural aspects of messenger RNA reading frame maintenance by the ribosome. *Nat. Struct. Mol. Biol.* **17**: 555-560.

Joung IS, Cheatham TE, 3rd. 2009. Molecular dynamics simulations of the dynamic and energetic properties of alkali and halide ions using water-model-specific ion parameters. *J. Phys. Chem. B* **113**: 13279-13290.

Khusainov I, Fatkhullin B, Pellegrino S, Bikmullin A, Liu WT, Gabdulkhakov A, Shebel AA, Golubev A, Zeyer D, Trachtmann N et al. 2020. Mechanism of ribosome shutdown by RsfS in Staphylococcus aureus revealed by integrative structural biology approach. *Nat. Commun.* **11**: 1656.

Klein DJ, Moore PB, Steitz TA. 2004. The contribution of metal ions to the structural stability of the large ribosomal subunit. *RNA* **10**: 1366-1379.

Kruse H, Sponer J, Auffinger P. 2019. Comment on "Evaluating Unexpectedly Short Non-covalent Distances in X-ray Crystal Structures of Proteins with Electronic Structure Analysis". *J. Chem. Inf. Model.* **59**: 3605-3608.

Leonarski F, D'Ascenzo L, Auffinger P. 2017. Mg^{2+} ions: do they bind to nucleobase nitrogens? *Nucleic Acids Res.* **45**: 987-1004.

-. 2019. Nucleobase carbonyl groups are poor Mg^{2+} inner-sphere binders but excellent monovalent ion binders - A critical PDB survey. *RNA* **25**: 173-192.

Liu Q, Liu Q, Hendrickson WA. 2013. Robust structural analysis of native biological macromolecules from multi-crystal anomalous diffraction data. *Acta Cryst.* **D69**: 1314-1332.

Miller-Fleming L, Olin-Sandoval V, Campbell K, Ralser M. 2015. Remaining mysteries of molecular biology: The role of polyamines in the cell. *J. Mol. Biol.* **427**: 3389-3406.

Minor W, Dauter Z, Helliwell JR, Jaskolski M, Wlodawer A. 2016. Safeguarding structural data repositories against bad apples. *Structure* **24**: 216-220.

Nierhaus KH. 2014. Mg^{2+}, K^{+}, and the ribosome. *J. Bacteriol.* **196**: 3817-3819.

Noeske J, Wasserman MR, Terry DS, Altman RB, Blanchard SC, Cate JH. 2015. High-resolution structure of the *Escherichia coli* ribosome. *Nat. Struct. Mol. Biol.* **22**: 336-341.

Pettersen EF, Goddard TD, Huang CC, Couch GS, Greenblatt DM, Meng EC, Ferrin TE. 2004. UCSF Chimera--a visualization system for exploratory research and analysis. *J. Comput. Chem.* **25**: 1605-1612.

Rozov A, Demeshkina N, Khusainov I, Westhof E, Yusupov M, Yusupova G. 2016. Novel base-pairing interactions at the tRNA wobble position crucial for accurate reading of the genetic code. *Nat. Commun.* **7**: 10457.

Rozov A, Khusainov I, El Omari K, Duman R, Mykhaylyk V, Yusupov M, Westhof E, Wagner A, Yusupova G. 2019. Importance of potassium ions for ribosome structure and function revealed by long-wavelength X-ray diffraction. *Nat. Commun.* **10**: 2519.

Shabalin IG, Porebski PJ, Minor W. 2018. Refining the macromolecular model - achieving the best agreement with the data from X-ray diffraction experiment. *Crystallogr. Rev.* **24**: 236-262.

Taylor R, Wood PA. 2019. A million crystal structures: The whole is greater than the sum of its parts. *Chem. Rev.*

Wagner A, Duman R, Henderson K, Mykhaylyk V. 2016. In-vacuum long-wavelength macromolecular crystallography. *Acta Cryst.* **D72**: 430-439.

Wang W, Zhao J, Han Q, Wang G, Yang G, Shallop AJ, Liu J, Gaffney BL, Jones RA. 2009. Modulation of RNA metal binding by flanking bases: ^{15}N NMR evaluation of GC, tandem GU, and tandem GA sites. *Nucleosides Nucleotides Nucleic Acids* **28**: 424-434.

Westhof E, Yusupov M, Yusupova G. 2019. The multiple flavors of GoU pairs in RNA. *J. Mol. Recognit.* **32**: e2782.

Zheng H, Chordia MD, Cooper DR, Chruszcz M, Muller P, Sheldrick GM, Minor W. 2014. Validation of metal-binding sites in macromolecular structures with the CheckMyMetal web server. *Nat. Protoc.* **9**: 156-170.

Zhou Y, Morais-Cabral JH, Kaufman A, MacKinnon R. 2001. Chemistry of ion coordination and hydration revealed by a K^{+} channel-Fab complex at 2.0 A resolution. *Nature* **414**: 43-48.

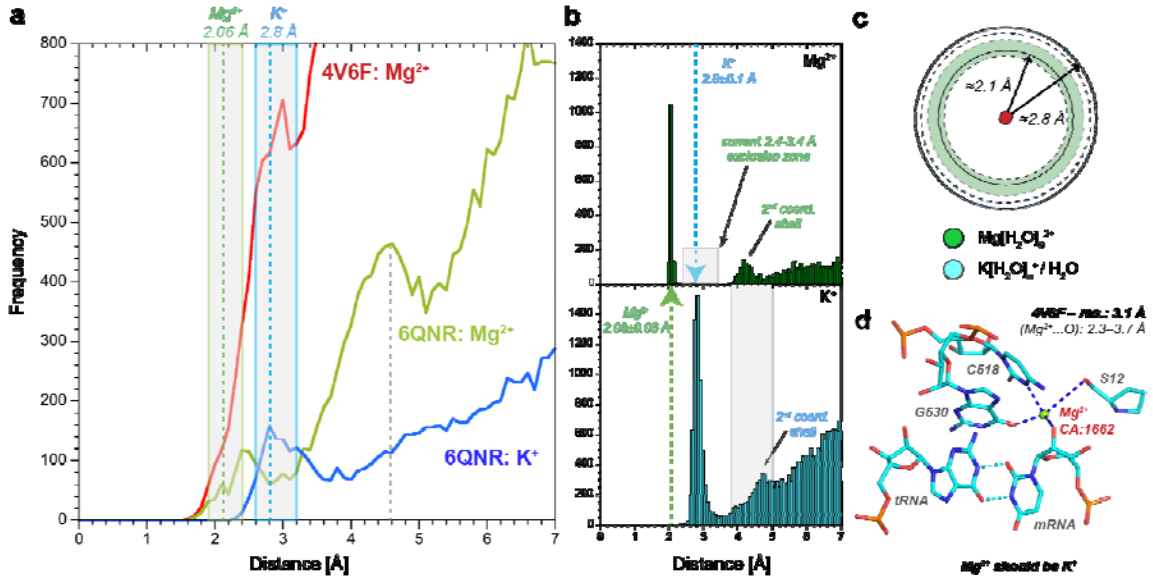

Figure 1. Mg^{2+} and K^+ coordination distances to oxygen atoms in 4V6F, 6QNR and the CSD. a The red, green and blue curves show the number of Mg^{2+} and K^+ bound to rRNA and r-protein oxygen atoms in the 4V6F (Jenner et al. 2010) and 6QNR (Rozov et al. 2019) structures. Water oxygens are excluded. The colored areas and the green and blue dashed lines highlight two regions where Mg^{2+} (1.9–2.4 Å; favored: 2.06 Å) and K^+ (2.6–3.2 Å; favored: 2.8 Å) should be present. The large 2nd peak in the green curve (≈4.6 Å) appears in a region where a precise ion assignment is problematic since it could correspond to the 2nd coordination shell of Mg^{2+} or to other solvent molecules, including K^+. **b** Cambridge Structural Database (CSD; Taylor and Wood 2019) histograms showing the Mg^{2+}…H_2O (green) and K^+…O (cyan) coordination distances. The 2nd coordination shell for K^+ and a H_2O "exclusion zone" for Mg^{2+}, where no oxygen atom is expected (grey areas). **c** Schematic representation of the respective 2.1 and 2.8 Å average coordination distances and 1.9–2.4 and 2.6–3.2 Å coordination range for Mg^{2+} and K^+ (see panel **b**). The white area between the green and blue segments (2.4–2.6 Å range) points to improper coordination distances for both Mg^{2+} and K^+. **d** View of the Mg^{2+} that has been assigned in the 4V6F decoding center (Rozov et al. 2016). An examination of the ion binding features suggests that this ion cannot be Mg^{2+} but is K^+ as assigned in 6QNR (Rozov et al. 2019) and by us in 5E81 (Leonarski et al. 2019). Density patterns for 6QNR and 5E81 are shown in **Figure S1**.

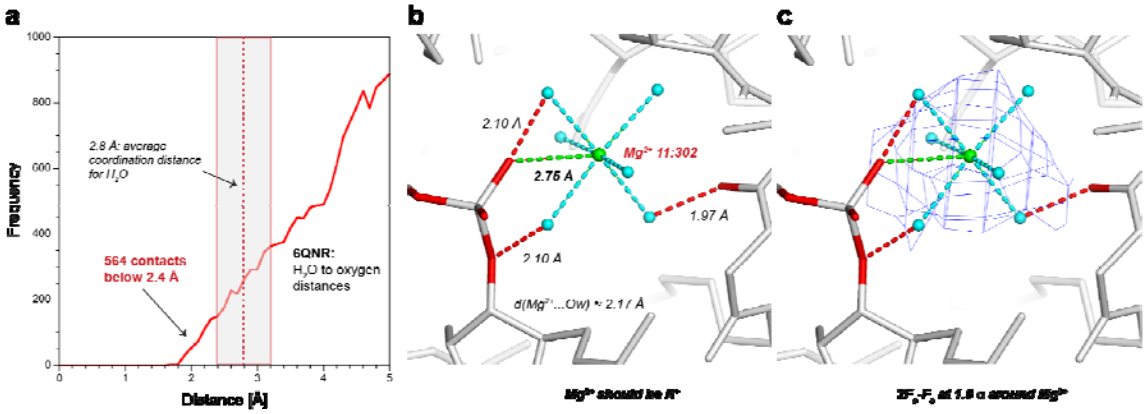

Figure 2. Abnormally short water to rRNA and r-protein contact distances reveal ill-placed Mg^{2+} in 6QNR. a The red curve shows the number of contacts between water molecules of the Mg^{2+} 1st hydration shell and rRNA and r-protein oxygen atoms with respect to distance. The 564 contacts < 2.4 Å reveal the presence of ill-placed Mg^{2+}. Note that the forgiving 2.4 Å hydrogen bond limit; a regular hydrogen bond is only exceptionally shorter than 2.5–2.6 Å (Kruse et al. 2019) and is more generally centered around 2.8 Å (grey box). **b** Example of a Mg^{2+} in 6QNR whose hydration sphere clashes with three oxygen atoms (red dashed lines; see also **Figure S4**). The 2.75 Å distance to a phosphate oxygen atom reveals unambiguously the presence of a K^+ (green dashed line). Note the average *d*(Mg^{2+}…Ow) distance close to 2.17 Å. **c** The corresponding $2F_o$-F_c map around the ion reveals no octahedral coordination pattern (**Figure S4**).

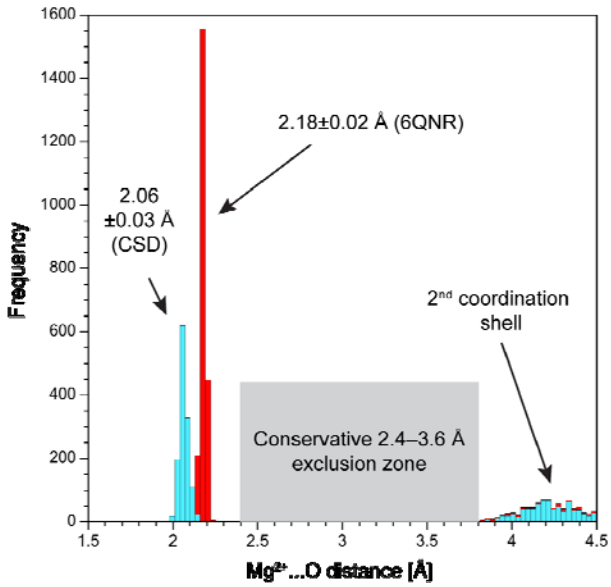

Figure 3. Mg^{2+}…O_w coordination distance bias towards 2.18 Å. The cyan histogram is derived from the CSD (Groom et al. 2016; Taylor and Wood 2019) and is similar to that in **Figure 1a**. The red histogram highlights the average Mg^{2+}…O_w distance around 2.18 Å in 6QNR (Rozov et al. 2019). These artefactual distances, common in PDB structures, have been discussed in preceding studies that provide also an exclusion zone definition (Leonarski et al. 2017; Leonarski et al. 2019), see also **Table S1** and **Figure 1**.

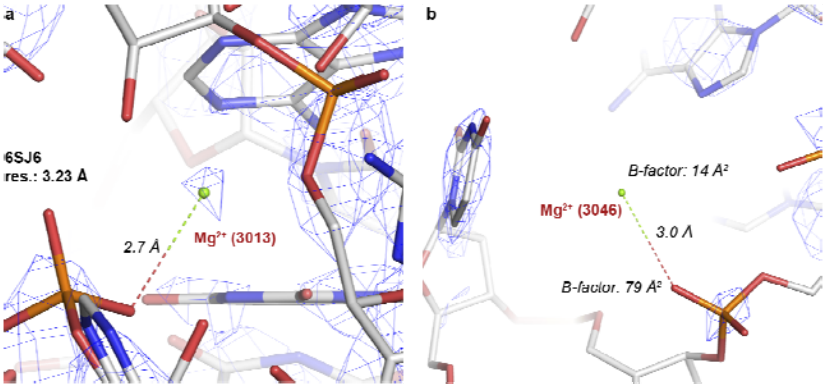

Figure 4. Two examples of improper Mg^{2+} assignments in the 6SJ6 cryo-EM structure (Khusainov et al. 2020). a The coordination distance to this ion excludes the presence of Mg^{2+} and rather suggests the presence of K^{+}. **b** As in (a). Note the large B-factor discrepancy.